Frontiers of Information Technology & Electronic Engineering
www.jzus.zju.edu.cn; engineering.cae.cn; www.springerlink.com
ISSN 2095-9184 (print); ISSN 2095-9230 (online)
E-mail: jzus@zju.edu.cn

*Review:*

# Channel measurements and models for 6G: current status and future outlook*

Jian-hua ZHANG†, Pan TANG†‡, Li YU, Tao JIANG, Lei TIAN

*State Key Lab of Networking and Switching Technology, Beijing University of Posts and Telecommunications, Beijing 100876, China*

†E-mail: jhzhang@bupt.edu.cn; tangpan27@bupt.edu.cn

Received Aug. 30, 2019; Revision accepted Dec. 22, 2019; Crosschecked Jan. 14, 2020

**Abstract:** With the commercialization of fifth generation networks worldwide, research into sixth generation (6G) networks has been launched to meet the demands for high data rates and low latency for future services. A wireless propagation channel is the transmission medium to transfer information between the transmitter and the receiver. Moreover, channel properties determine the ultimate performance limit of wireless communication systems. Thus, conducting channel research is a prerequisite to designing 6G wireless communication systems. In this paper, we first introduce several emerging technologies and applications for 6G, such as terahertz communication, industrial Internet of Things, space-air-ground integrated network, and machine learning, and point out the developing trends of 6G channel models. Then, we give a review of channel measurements and models for the technologies and applications. Finally, the outlook for 6G channel measurements and models is discussed.

**Key words:** Channel measurements; Channel models; Sixth generation; Terahertz; Industrial Internet of Things; Space-air-ground integrated network; Machine learning

https://doi.org/10.1631/FITEE.1900450 **CLC number:** TN929.5

## 1 Introduction

Commercialization of fifth generation (5G) networks is being carried out worldwide. Furthermore, the third Generation Partnership Project (3GPP) Release 16 is "5G phase 2" and will be frozen in 2020, which will meet International Mobile Telecommunications (IMT)–2020 submission requirements of the International Telecommunication Union (ITU). However, with the development of big data, the Internet, cloud computing, smart city, and integration of multidimensional networks, the data traffic has grown continually. ITU has already estimated the traffic for the years 2020–2030 (ITU-R, 2015). It is forecast that the number of global mobile subscriptions could reach 13.8 billion in 2025 and 17.1 billion in 2030. Furthermore, the global mobile traffic per month, including machine to machine (M2M) traffic, is estimated to reach 607 exabytes (EB) in 2025 and 5016 EB in 2030, although it is only 62 EB in 2020 (Fig. 1). This may be beyond the bearing capacity of the 5G networks. From fourth generation (4G) to 5G, the peak data rate increases from the order of megabit/s (Mb/s) to gigabit/s (Gb/s), and the sixth generation (6G) is expected to achieve terabit/s (Tb/s) data rate to meet the challenge of continually increasing traffic (CMRI, 2019; Zhang P et al., 2019).

With the commercialization of 5G networks worldwide, some countries and organizations have

‡ Corresponding author

* Project supported by the National Key R&D Program of China (No. 2018YFB1801101), the National Science Fund for Distinguished Young Scholars, China (No. 61925102), the Key Project of State Key Lab of Networking and Switching Technology, China (No. NST20180105), Huawei, and ZTE Corporation

ORCID: Jian-hua ZHANG, https://orcid.org/0000-0002-6492-3846; Pan TANG, https://orcid.org/0000-0003-0432-7361

started to research on 6G. In September 2017, the European Union started projects to research terahertz (THz) communication, visible light communication, and D band radio for beyond 5G (B5G). In 2018, the University of Oulu's "6Genesis-6G-Enabled Wireless Smart Society & Ecosystem" project was chosen as one of the first two flagships in a national research program funded by the Finnish government. In July 2018, the ITU-T Focus Group Technologies for Network 2030 (FG NET-2030) was established, intended to study the capabilities of networks for the year 2030 and beyond. In December 2018, several communication companies in China, including China Mobile Communications Corporation (CMCC), Huawei, and Oppo, started a project called the "Vision and Need of B5G Systems." In March 2019, the Federal Communications Commission (FCC) opened up experimental spectrum licenses for 6G. In June 2019, it was announced that Korea Telecom (KT) and Seoul National University would cooperate in developing and standardizing technologies for 6G telecommunications. Moreover, the Electronics and Telecommunications Research Institute (ETRI) signed a memorandum of understanding with the University of Oulu in Finland to develop 6G network technology. In November 2019, the Ministry of Science and Technology announced that China has established a national research and development group for 6G.

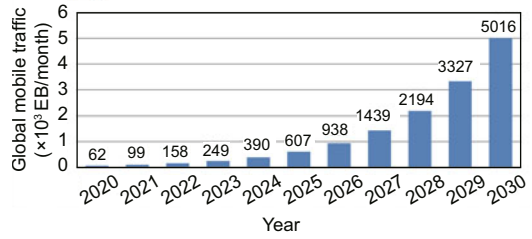


**Fig. 1 Estimations of global mobile traffic in 2020–2030 (M2M traffic included) (ITU-R, 2015)**

The wireless propagation channel is the medium, linking the transmitter (Tx) and the receiver (Rx), and channel properties determine the ultimate performance limit of wireless communications (Molisch, 2012). Channel properties are usually classified into large-scale fading and small-scale fading. Large-scale fading is a significant reduction in signal strength on a large scale (typically, a few hundred wavelengths), including path loss and shadow fading. Path loss determines the coverage area of a base station (BS) and is helpful for BS deployment (Richter et al., 2009). Small-scale fading is the rapid fluctuation of signal strength on a small scale that is comparable with a single wavelength, including delay spread (DS) and angular spread. Furthermore, small-scale fading is the fading of channel in space-time-frequency multidimensional domains, which greatly influences the air interface transmission techniques. For example, DS can be used to design the cyclic prefix to deal with the inter-carrier interference in orthogonal frequency division multiplexing (OFDM) systems (Liu XQ et al., 2017). Accordingly, we can see that research on channel properties is a prerequisite to designing 6G wireless communication systems. The 3GPP and ITU groups have issued several channel model standards for 5G, such as ITU M.2412 (WP5D I, 2017), 3GPP Technical Report (TR) 38.900 (Meredith, 2016), and 3GPP TR 38.901 (3GPP, 2018). They are the foundations for the performance evaluation of technologies and communication systems. New technologies and applications, such as THz wave communication, space-air-ground integrated network (SAGIN), and machine learning (ML), have been proposed for 6G (CMRI, 2019; Zhang P et al., 2019), and they have challenging requirements for channel models. Accordingly, 6G channel models should support a wide range of frequencies, up to THz bands, and various scenarios. Details about requirements and developing trends of 6G channel models are discussed in Section 2.

To date, some research organizations have conducted channel measurements and proposed new channel models for the above-mentioned technologies and applications. In Priebe et al. (2011), ultra-broadband channel measurements at 300 gigahertz (GHz) were presented, and path loss, delay, and spatial characteristics were analyzed. Liu L et al. (2018) investigated channel propagation characteristics based on the field measurement data in an automobile factory. In other works (Matolak and Sun, 2017a, 2017b; Sun and Matolak, 2017), a series of air-to-ground channel measurements for most of the typical ground site-local environments were presented, and channel models based on measurements were provided. In Zhang J (2016), a cluster-nuclei based channel model was proposed based on ML. More reviews can be found in Section 3.

To the best of our knowledge, there has been no review paper for 6G channel measurements and models. This paper aims to provide a review of the present 6G channel measurements and models and present the outlook for future research. The main contributions of this paper are listed as follows:

1. New technologies and applications for 6G are introduced. Based on analysis of requirements of these technologies and applications, the developing trends of 6G channel models are presented.

2. A review of 6G channel measurements and models is given in terms of different technologies or applications for 6G. Specific channel characteristics and modeling methods are discussed which should be considered in channel modeling for 6G.

3. Combining the review of 6G channel measurements and models with a discussion on the developing trends of 6G channel models, the outlook for future research on channel measurements and models is discussed.

## 2 Developing trends of channel models for 6G

The development of past cellular generations has always been driven by new services and applications. For 5G applications, the systems need to support high data rate (20 Gb/s peak data rate), a large number of connected devices (1 million devices/km$^2$), and ultra-low latency (1 ms) (Series, 2015). Moreover, 5G systems aim to provide anywhere and anytime connectivity for anyone and anything (Dahlman et al., 2014). Though this goal has not been fully achieved until now, new applications have been proposed which drive 6G systems toward development. For example, holographic communications should provide new forms of interaction and lead to a true immersion into a distant environment (Strinati et al., 2019). High-precision manufacturing needs 0.1–1 ms round trip time and high reliability (Berardinelli et al., 2018). Three-dimensional (3D) coverage needs an integrated network that terrestrial equipment, airborne equipment, and satellites can all access. To enable emerging applications and guarantee their performance, new technologies for 6G are needed. Technologies bring new trends of channels and then cause challenges in channel modeling.

### 2.1 New technologies and applications for 6G

ITU has estimated the global mobile traffic for the next 10 years (ITU-R, 2015). However, available technologies that can meet the challenge of high volumes of traffic have not been clearly defined by 3GPP yet. Based on the projects launched and academic publications, we can summarize several emerging technologies and applications.

#### 2.1.1 Terahertz wireless communication

Frequency is an extremely valuable and limited resource for wireless communication. Since the low-frequency bands (below 6 GHz) are dramatically crowded, looking for available spectrum in the higher-frequency bands has started in the 5G era (Zhang JH et al., 2017a). Several millimeter-wave (mm-wave) bands (between 6 and 100 GHz) have been granted for 5G due to the potential of wide and continuous spectrums to support the 5G goal of 20 Gb/s peak data rate. According to the prediction report by Cisco Visual Networking Index (VNI) in February 2019, the global data traffic over the period of 2017–2022 is growing at the speed of 46% per year, driven by various new services such as virtual reality (VR), augmented reality (AR), ultra-high-definition (UHD) video, and holographic video (Cisco, 2019). For instance, the transmission of an uncompressed UHD video might reach 24 Gb/s, and the transmission of an uncompressed 3D high-quality holographic video can increase up to nearly 100 Gb/s. It can be foreseen that the data rate requirement could reach 1 Tb/s in the next 10 years. It is still a challenge to use spectrums in bands below 100 GHz to support the Tb/s data rate. However, in THz bands (between 0.1 and 10 THz), more available spectrum sources can be used for communications. In the World Radiocommunication Conference 2019 (WRC-19), the 275–296, 306–313, 318–333, and 356–450 GHz bands were identified for unrestricted use in fixed service and land mobile applications. From Table 1, we can see that there are totally 137 GHz bandwidths available. This indicates that THz wireless

**Table 1 Identified THz bands in WRC-19**

| Frequency range (GHz) | Contiguous bandwidth (GHz) |
|---|---|
| 275–296 | 21 |
| 306–313 | 7 |
| 318–333 | 15 |
| 356–450 | 94 |

communication is a promising way to achieve Tb/s transmission for 6G.

### 2.1.2 Industrial Internet of Things

Compared with 4G, the connection density in the 5G era increases by 10 times. It is predictable that the connection density will grow further in the 6G era. This provides more opportunities for building a new network named the Industrial Internet of Things (IIoT). As shown in Fig. 2, it connects massive industrial devices and results in systems that can monitor, collect, exchange, analyze, and deliver the valuable new insights like never before. It collects real-time data from the sensors and uploads them to the cloud in a timely and rapid manner. This demands an extra-high data rate and an extra-low latency. Moreover, 6G can provide a data rate of 1 Tb/s and a latency of 0.1 ms to support the application of IIoT (Strinati et al., 2019). Furthermore, networks in 5G are individually smart, while 6G can have integrated smart networks (Zhang P et al., 2019). This helps realize the smart factory as a concept. To enable communication between the massive IIoT devices and the present Long-Term Evolution (LTE) network, 3GPP has established four enhanced standards: LTE category 1, LTE category 0, LTE category M1, and LTE category M2 (which is also named narrow-band IoT). They are driving the growth of the number of cellular IoT connections worldwide. It is expected that by 2024, there would be 4.1 billion cellular IoT connections (Cerwall et al., 2015).

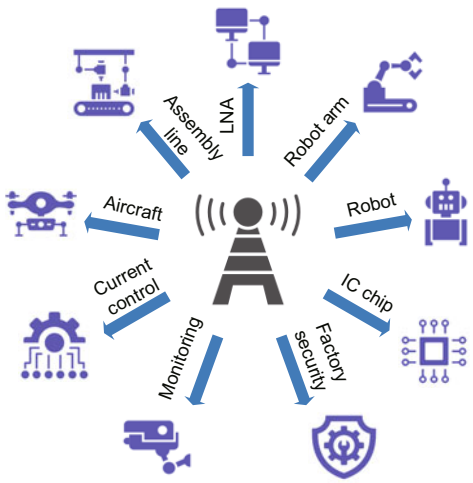


**Fig. 2 The application scenarios of IIoT**

### 2.1.3 Space-air-ground integrated network

In a traditional cellular network, communications usually happen between terrestrial equipments, e.g., mobile phones, stations, and cars. The usage scenarios for 5G can be classified as enhanced mobile broadband (eMBB), ultra-reliable and low latency communications (uRLLC), and massive machine type communications (mMTC) (Series, 2015). As the development of science and technologies, more and more devices need to access the communication network to support new applications. Unmanned aerial vehicles (UAVs) can transmit data, e.g., images, videos, and control commends, to a console through the communication network. Furthermore, human activity space is rapidly expanding. Not only scientists but also the ordinary person would like to explore the outer space. Thus, the need for communication between satellites and the ground will be more prevalent. However, the current wireless communication network has a limited coverage. It can provide services for only 70% of humans. Besides, it covers only about 20% of the land area, which is less than 6% of the Earth's surface area. To satisfy the need for communication in wider space, 6G may be a SAGIN that is an integration of satellite systems, aerial networks, and terrestrial communications (Fig. 3). SAGIN can provide pervasive coverage and bring significant benefits for various practical services and applications, but many challenges, e.g., heterogeneity, self-organization, and time-variability, should be overcome due to its specific characteristics (Liu JJ et al., 2018).

### 2.1.4 Machine learning

Motivated by big data and artificial intelligence, there has been a recognition that increasing requirements brought by 5G need to be satisfied by an intelligent network. The extensive enhancement of the capacity of communication networks and the increasingly smart mobile devices have produced an eruption of new applications which will be used for mobile connectivity and the resultant exponential growth in network traffic. A new ITU standard, ITU Y.3172, has established a basis for the cost-effective integration of ML into 5G and future networks (ITU-T, 2019). ML, as one of the most powerful artificial intelligence tools, has been dramatically developed over the past few years. It has been widely applied

in image/audio processing, finance and economics, social behavior analysis, and project management (Joo and Zhou, 2009). Recently, some attempts have been made to apply ML to the area of wireless communication systems. In Li W et al. (2019), a three-layer structure of wireless channel fading was proposed to classify the versatile propagation environments. Based on this structure, some feasible ways to combine ML with the wireless network are summarized in Fig. 4. Jiang et al. (2016) also discussed the applications of ML in 5G. As the traffic explosively grows in B5G, a huge amount of data is created and needs to be processed in a timely manner. Moreover, with the growth of the number of access points and users, 6G deployments will be denser and 6G air interfaces will be more complicated (Giordani et al., 2019; Shafin et al., 2019). This results in the significant increase in network complexity. In this case, using ML in wireless communications becomes more necessary.

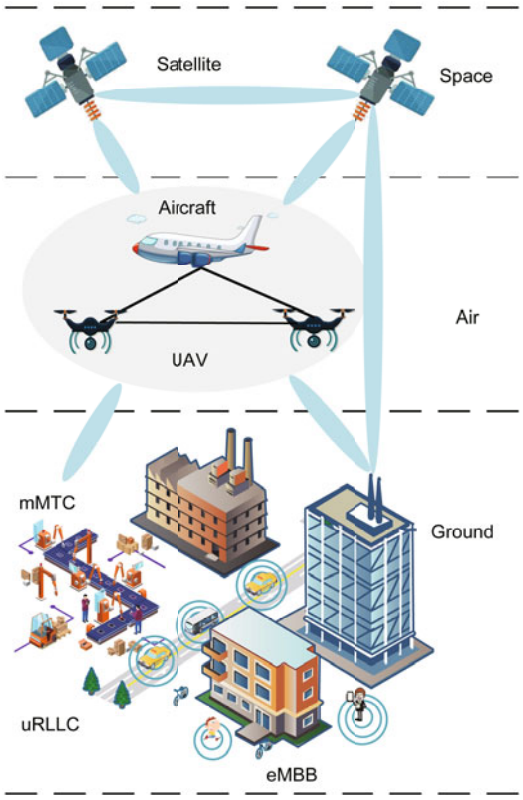


**Fig. 3 Diagram of a SAGIN**

## 2.2 Challenges in channel modeling for 6G

With the emergence of new technologies and applications, there are three new trends of the radio channel: higher frequencies, larger scale of antenna arrays, and more diverse wireless communication scenarios. Fig. 5 explains the evolution from 5G to 6G in terms of these three trends. These new properties challenge traditional channel models.

### 2.2.1 Higher frequency and wider bandwidth

Millimeter-wave technology is one of the key technologies of 5G because mm-wave bands have continuous and wide spectrums (Rappaport et al., 2017). In WRC-15, some mm-wave bands below

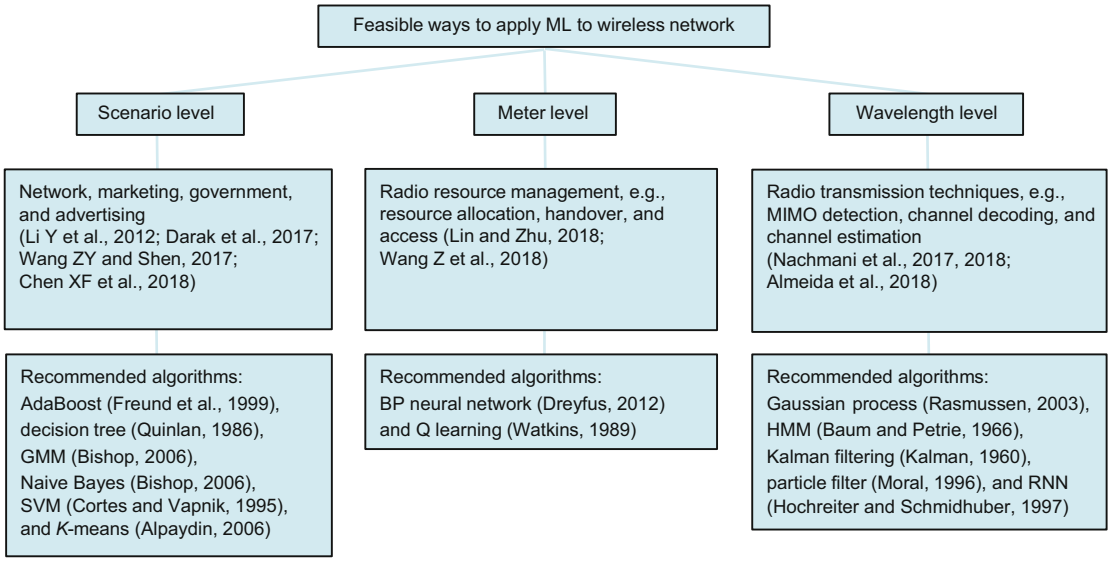


**Fig. 4 Machine learning applications in 5G from the channel perspective**

100 GHz were considered as potential candidate bands for 5G, such as 66–76 GHz bands with a bandwidth of 10 GHz. In WRC-19, ITU added more mm-wave bands, i.e., 24.25–27.5, 37–43.5, 45.5–47, 47.2–48.2, and 66–71 GHz. Furthermore, the channel model standards issued by 3GPP and ITU support the modeling of channels up to 100 GHz. Demands for higher data rates drive people to use higher frequency and wider bandwidth for 6G. As the frequency increases, the wavelength becomes smaller and the propagation characteristics may have obvious changes compared to the low frequency wave. For example, radio waves in the THz bands suffer from absorption or scattering by molecules and tiny particles in the atmosphere, such as water vapour and oxygen, because their sizes are close to the wavelength of the THz wave. As Fig. 6 shows, the total attenuation caused by air and water vapor is about $1.98\times10^5$ dB/km at 558 GHz, while it is only about 0.01 dB/km at 6 GHz (ITU-R, 2013). Furthermore, the reflection or diffraction by obstacles in the THz bands shows certain unique behaviors compared with

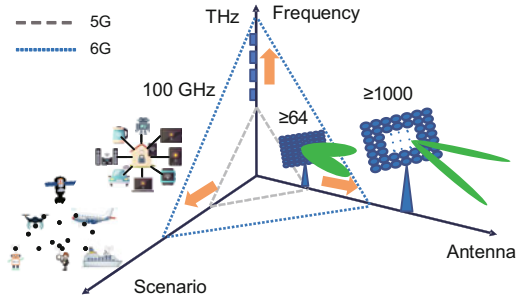


**Fig. 5 The evolution trends of channel properties from 5G to 6G**

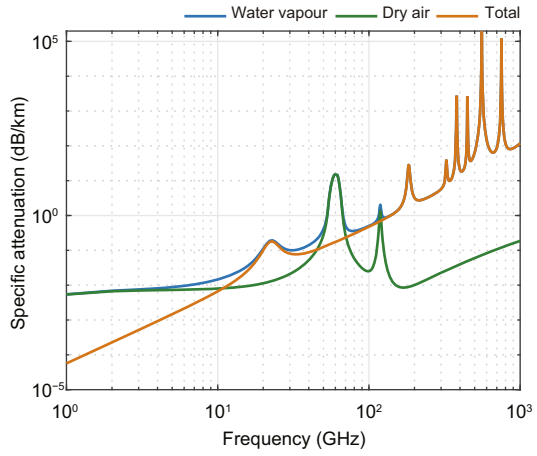


**Fig. 6 Specific attenuation due to atmospheric gases (ITU-R, 2013)**

that in the low-frequency bands due to the smaller wavelength. The THz channel is more likely to be sparse due to the weak diffraction ability. These make current channel models unavailable. Moreover, considering the high cost of building a wideband and high-frequency channel sounder (CS), obtaining reliable and extensive channel information using a CS from the higher-frequency and wider-band channels is challenging.

### 2.2.2 Ultra-large-scale antenna arrays

Multiple-input-multiple-output (MIMO) technology has been widely used in wireless communication systems, and it has been demonstrated that it can achieve greater performance enhancements (Goldsmith et al., 2003). As the radio frequency increases, it is possible to build larger-scale antenna arrays because smaller spacing between adjacent antennas can be achieved. Marzetta (2010) first proposed to equip BSs with massive MIMO antenna arrays to serve users, which can bring good performance gain (Liu GY et al., 2016). Furthermore, the system capacity can be improved using 3D antenna arrays (Zhang J et al., 2014; Liu GY et al., 2016). Based on channel measurements, 3D MIMO technologies have been verified to achieve 33% gain in channel capacity compared with 2D MIMO technologies in outdoor to indoor (O2I) scenarios (Zhang JH et al., 2017b). As the number of antennas increases, the 3D MIMO channel becomes dispersive in the spatial domain, which leads to a remarkable improvement of channel capacity (Zhang JH et al., 2018). Thus, massive MIMO technology is another key technology of 5G (Ali et al., 2017; Li JZ et al., 2017). For 6G, as the frequency continues to increase, ultra-large-scale antenna arrays can be used. Though it seems to be promising, modeling the channel with ultra-large-scale antenna arrays becomes challenging. Measurements using a virtual 40×40 planar antenna array have been previously presented (Chen JJ et al., 2017). Measurement results show that channel properties are non-stationary over the array. For example, Fig. 7 shows that the Rice factor (also called the $K$-factor) gradually changes across the large-scale antenna array aperture. Thus, non-stationarity across the antenna array should be considered in channel modeling. Furthermore, more antennas give rise to narrower beams (Zhang JH et al., 2018). Thus, more accurate channel parameters,

e.g., angles of multipath components (MPCs), are needed to make beams precisely point to users. From the channel measurement point of view, it is challenging to use ultra-large-scale antenna arrays to conduct channel measurements. On one hand, it is hard to apply large-scale antenna arrays in the CS, especially in the THz bands. On the other hand, the measured data volume exponentially increases with the increase of the scale of antenna arrays, and more computing cost, e.g., in data preprocessing and channel state information extraction, is needed.

#### 2.2.3 Diverse application scenarios

As shown in Fig. 8, the usage scenarios for 5G fall into three categories: eMBB, uRLLC, and mMTC (Series, 2015). These scenarios almost cover wireless communication on the ground. However, as wireless communication technologies develop and demands for communication in larger-scale space increase, a space-air-ground wireless communication system is needed for 6G. Fig. 3 shows the diagram of a SAGIN. In this network, communication happens between satellites, aircrafts, UAVs, ground stations, things, and users. In this case, wireless communication channels become extra complex and diverse. Moreover, obtaining the channel characteristics by channel measurement operations in all scenarios is probably impossible.

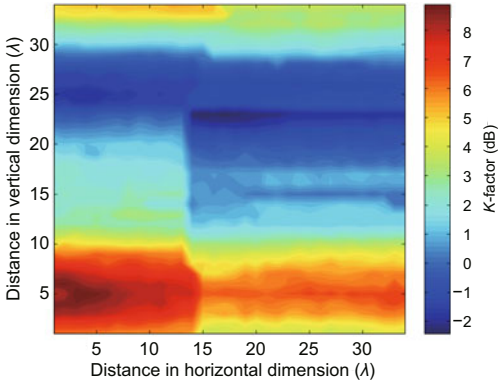


**Fig. 7 *K*-factor values observed across the antenna array**

Reprinted from Chen JJ et al. (2017), Copyright 2017, with permission from IEEE

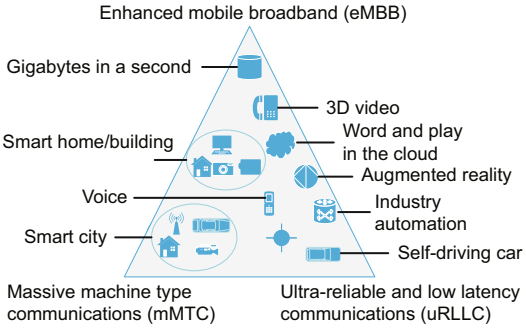


**Fig. 8 Usage scenarios of 5G (Series, 2015)**

## 3 Current status of channel measurements and models for 6G

In the foregoing text, we have discussed that research on channels is crucial to the design of wireless communication systems. Furthermore, emerging technologies and applications bring in new trends of channels for 6G. Until now, a number of research organizations have conducted channel measurements and proposed new channel models for 6G. Here, we summarize the state of the art of 6G channel measurements and models considering different 6G communication technologies and applications.

### 3.1 Terahertz channel measurements and models

As shown in Fig. 9, there is a trend toward using higher-frequency bands, THz bands, for 6G. The THz bands are located between mm-wave and infrared waves. With the increase in the frequency, radio wave propagation is influenced significantly by the absorption and diffraction by the molecules in the air (ITU-R, 2013). The THz wave might behave uniquely compared with the lower band. Knowledge of the THz channel is one of the most important issues to be addressed for the future THz communication system.

Conducting channel measurements is a widely used method for researching channel properties. Most of the reported THz channel measurements

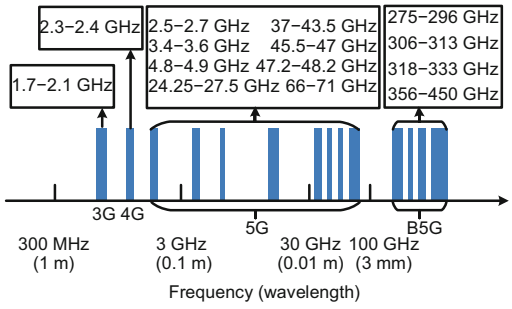


**Fig. 9 Bands used for mobile communications**

are conducted by the THz time-domain spectroscopy (TDS) and vector network analyzer (VNA). The THz-TDS system, which works by converting the ultra-short optical pulse to a THz radiation pulse, was first developed for THz imaging applications in Hu and Nuss (1995) and used to measure the electrical and scattering parameters of a material. VNA, which works in the frequency domain, is widely used in radio channel measurements, especially for high frequencies such as mm-wave bands, due to the easy setup and the inherent synchronization between Tx and Rx (Lei et al., 2015). However, limited by the highest frequency of VNA, a pair of up/down frequency converters cooperating with a four-port VNA was used to conduct channel measurements on certain THz bands in Priebe et al. (2011). In addition, a correlation-based CS was built using different frequency extensions (Rey et al., 2017). This CS supports $2\times2$ MIMO at 60 GHz and 300 GHz and has a bandwidth of up to approximately 8 GHz.

The recent THz channel measurements can be roughly categorized into two kinds. The first kind focuses on the effect of the THz propagation mechanism on different materials or obstacles such as reflection and diffraction. In Piesiewicz et al. (2005), the reflective properties were studied at different angles from 75 to 300 GHz using THz-TDS. Three typical building materials, namely, window glass, plaster, and pinewood, were considered. From the results, it was interpreted that the scattering losses of the material surface can be neglected. The reflection properties of two kinds of stratified building materials were measured by THz-TDS in the frequency range from 100 to 500 GHz for a set of angles (Jansen et al., 2008). The reflectivity of materials with a rough surface was modeled using the Kirchhoff scattering theory, based on the measurement of reflection from ingrain wallpaper and concrete plaster from 0.1 to 1 THz using THz-TDS (Jansen et al., 2011). In another study (Jacob et al., 2012), extensive measurements of the diffraction from objects, such as edges, wedges, and cylinders, were conducted at 60 GHz and 300 GHz by VNA. The human body and different materials, such as metal and wood, were taken into account in the measurements. The knife-edge model and the uniform geometrical theory of diffraction were found to agree with the measurement results well. Furthermore, using a validated ray-tracing tool, it was found that the diffraction at edges or wedges could be neglected almost everywhere in a room.

The second kind of THz channel measurements is dedicated to the traditional channel parameters in THz bands, such as path loss, delay, and even spatial characteristics. Priebe et al. (2011) conducted ultra-broadband channel measurement at 300 GHz with a 10 GHz sweeping span using a VNA and high-directive antennas for two indoor communication links, namely, a device-to-device link on a desktop and a link between a laptop and an access point in the middle of an office. Furthermore, the channel transfer function, path loss, and root-mean-square (RMS) DS were analyzed. The close-in (CI) path loss model was used to fit the measurement results as

$$\mathrm{PL}(d)[\mathrm{dB}]=\mathrm{PL}(d_0)+10n\lg\left(\frac{d}{d_0}\right)+X_\sigma, \quad (1)$$

where $d\geq d_0$, $d_0$ is the reference distance (usually $d_0=1$), $\mathrm{PL}(d_0)$ is the path loss at the distance of $d_0$, $d$ denotes the module distance, $n$ is the path loss exponent, and $X_\sigma$ models the shadow fading. The fitted path loss exponent is 2.17, which is a little larger than that of the free-space model (Fig. 10). RMS DS of the best direction alignment ranged from 16.5 to 127 ps. In Kim and Zajić (2015), measurements and statistical characterization of 300-to-320 GHz desktop channels were presented. It was found that the path loss exponent was around 1.9. In Cheng CL et al. (2017), different path loss modeling methods were investigated and compared based on an extensive measurement at 30, 140, and 300 GHz. Results showed that the multi-frequency model was more stable than the single-frequency model. A $2\times2$

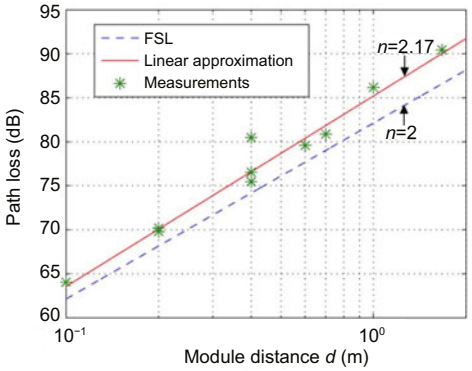


**Fig. 10 Indoor path loss averaged between 300 and 310 GHz**

Reprinted from Priebe et al. (2011), Copyright 2011, with permission from IEEE

virtual MIMO channel measurement carried out at 300 GHz with a 50 GHz sweeping frequency span in a 4.5 m×3.6 m small indoor office scenario was presented in Priebe et al. (2013). The measurement resolutions of delay and angle were 0.2 ns and 2°, respectively. The measured RMS DS ranged from 2 to 3.7 ns, and the angular spread of departure ranged from 18.3° to 37° in different Tx locations. In Pometcu and D'Errico (2018), large-scale and cluster characteristics were analyzed based on a VNA measurement from 126 to 156 GHz in three typical indoor environments (laboratory, conference room, and office room). The path loss exponent was 1.45 in the laboratory, whereas it was about 1.9 in the conference and office rooms. The median value of cluster DS was below 10 ns in all three environments. The channel transfer function was measured from 260 to 400 GHz in a short-range desktop environment for both line-of-sight (LoS) and reflected non-line-of-sight (NLoS) conditions, and the capacity was analyzed to show that Tb/s throughput was achievable in the THz bands (Khalid and Akan, 2016).

Regarding the current research on THz channel modeling, most studies adopt ray-tracing methods. In Priebe et al. (2014), ray-tracing was used for the simulation of THz radio wave propagation to analyze the distance-dependent behavior of angular spread and DS. In Priebe and Kuerner (2013), a stochastic indoor channel model at 300 GHz was introduced, the model parameters of which were derived from the ray-tracing simulations in an office scenario. The performance of the future multigigabit system was investigated based on a ray-tracing THz indoor channel simulation taking LoS, as well as single and double bounce reflection, into account (Piesiewicz et al., 2008). In Table 2, a summary of these channel measurements at the THz range is provided.

### 3.2 IIoT channel measurements and models

IIoT channel measurements were conducted mainly in sub-6 GHz bands, e.g., 1.35 GHz (Hanssens et al., 2018), 2.4 GHz (Miaoudakis et al., 2005), and 5.85 GHz (Luo et al., 2011). Recently, some measurements were also made in mm-wave bands, e.g., 54 and 70 GHz (Raimundo et al., 2018). The typical measurement scenarios of IIoT include the factory, warehouse (Hanssens et al., 2018), and industrial robots (Holfeld et al., 2016). Compared with conventional indoor scenarios, they have a larger size and a higher ceiling (Fig. 11). Moreover, there are many metal objects in the IIoT environment and

**Table 2 Recent channel characterization studies at the THz range**

| Reference | Frequency (GHz) | Equipment | Scenario | Channel characteristics |
|---|---|---|---|---|
| Piesiewicz et al. (2005) | 75–100 | THz-TDS | Building materials: window glass, plaster, and pine wood | Reflection |
| Jansen et al. (2008) | 100–500 | THz-TDS | Stratified building materials | Reflection |
| Jansen et al. (2011) | 100–1000 | THz-TDS | Rough surface materials | Reflection and scattering |
| Priebe et al. (2011) | 300–310 | VNA | Desktop and indoor office | Channel transfer function, path loss, delay, and angle |
| Jacob et al. (2012) | 275–325 | VNA | Metal and wood edges, wedges, and cylinders | Diffraction, ray-tracing for path loss, delay, and impact of objects |
| Priebe et al. (2013) | 275–325 | VNA | Indoor office | Angular spread of arrival and departure |
| Kim and Zajić (2015) | 300–320 | VNA | Desktop | Path loss, shadow fading, and delay |
| Khalid and Akan (2016) | 260–400 | VNA | Desktop | Channel transfer function and capacity |
| Cheng CL et al. (2017) | 140, 300 | VNA | Indoor room | Path loss |
| Pometcu and D'Errico (2018) | 126–156 | VNA | Laboratory, conference room, and office room | Path loss, delay, angle, and cluster |
| Piesiewicz et al. (2008) | 350 | – | Indoor office | Ray-tracing and data rate |
| Priebe and Kuerner (2013) | 275–325 | – | Indoor office | Stochastic model and parameter from ray-tracing data |
| Priebe et al. (2014) | 300 | – | Indoor room | 3-D ray-tracing, angle, and delay |

their smooth surfaces make the number of reflection paths increase. The most obvious effect of the channel model is the increase of DS and the decrease of path loss.

**Fig. 11 Real industrial environment**

In the case of highly reflective environments, MPCs arrive more than 1000 ns after the first arriving component. However, in a high-absorbent environment, the maximum excess delay is around 30 ns, which is far smaller than that in the highly reflective environments (Ferrer-Coll et al., 2012). In a manufacturing-like environment (Miaoudakis et al., 2005), 50% of values exceed 83 ns for the average delay and 72 ns for RMS DS. Furthermore, 73% of the RMS DS values are between 60 and 90 ns. In a chemical production factory, RMS DS ranges from 28 to 38 ns for the LoS case and from 34 to 51 ns for the NLoS case. In a MAX-Lab, RMS DS ranges from 34 to 45 ns for the NLoS case (Karedal et al., 2007). In a machine room, RMS DS varies from 133 to 153 ns in the LoS case, and from 177 to 201 ns in the NLoS case (CMCC and BUPT, 2018a). However, at the same frequency, RMS DS is only 20 ns and 41 ns in the LoS and NLoS cases in the indoor office, respectively.

In the meantime, the rich reflection paths slow down the increase of path loss in the LoS case. The exponent of path loss is 2 in the free-space, but it is always lower than 2 in the factory environment. In the machine shop, the exponent varies from 1.1 to 1.4 at 4.9 GHz (CMCC and BUPT, 2018b). In the industrial facility, the exponent is 1.6 at 2.4 GHz (Sexton et al., 2005). When the multifrequency measurements are synthesized, the exponent increases to 1.9, but it is still less than the free-space value (Huawei and HiSilicon, 2018). As for the NLoS case, the exponent ranges from 1.9 to 3.8, and it is often smaller than that in the indoor scenario in 3GPP TR 38.901 (3GPP, 2018). Furthermore, the first arriving component is strong even in NLoS situations when the distance between Tx and Rx is small. Moreover, the path loss increases with the increase of the frequency (Liu L et al., 2018).

The LoS probability is another important channel characteristic that changes in the IIoT scenario. According to 3GPP TR 38.901 (3GPP, 2018), the LoS probability is derived by assuming that the antenna height is 3 m in indoor scenarios. However, in the IIoT scenario, the height of the ceiling is always higher than 10 m (5G-ACIA, 2018). In addition, clutter density is introduced in the modeling of the LoS probability. In the heavy industry scenario, the larger equipment and the greater number of metallic objects become the main sources of blockage. The light industry layout consists mostly of open space, where human bodies become the sources of blockage and the average height is 1.5 m. As shown in Fig. 12, the previous channel model is unable to describe the LoS probability. The LoS probability for heavy industry decays more rapidly in contrast to that for light industry, as the Tx-Rx distance increases (Solomitckii et al., 2018).

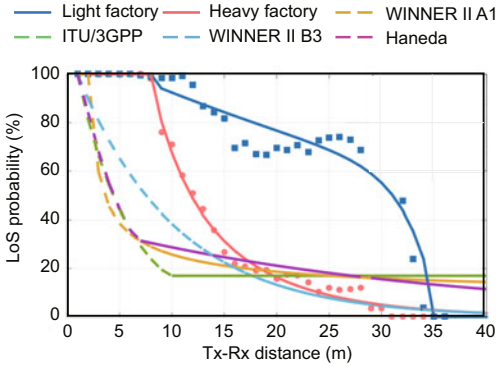


**Fig. 12 LoS probability for light and heavy industry**
Reprinted from Solomitckii et al. (2018), Copyright 2018, with permission from IEEE

Apart from the conventional channel properties mentioned herein, two other properties, the dual mobility and the absolute time of arrival, are also important in the control channel of automatic guided vehicles (AGVs) and movable robots in IIoT scenarios. The new proposal (Ericsson, 2019b) recommended applying the dual mobility model in 3GPP TR 37.885 (3GPP, 2019). The Doppler shift

for the LoS path can be written as

$$\boldsymbol{\nu}_{n,m}=\frac{\hat{\boldsymbol{r}}_{rx,n,m}^{\mathrm{T}}\bar{\boldsymbol{\nu}}_{rx}+\hat{\boldsymbol{r}}_{tx,n,m}^{\mathrm{T}}\bar{\boldsymbol{\nu}}_{tx}}{\lambda_0}. \tag{2}$$

The Doppler shift for delayed paths can be written as

$$\boldsymbol{\nu}_{n,m}=\frac{\hat{\boldsymbol{r}}_{rx,n,m}^{\mathrm{T}}\bar{\boldsymbol{\nu}}_{rx}+\hat{\boldsymbol{r}}_{tx,n,m}^{\mathrm{T}}\bar{\boldsymbol{\nu}}_{tx}+2\alpha_{n,m}D_{n,m}}{\lambda_0}, \tag{3}$$

where $D_{n,m}$ is a random variable with a uniform distribution from $-\nu_{\mathrm{scatt}}$ to $\nu_{\mathrm{scatt}}$, $\nu_{\mathrm{scatt}}$ is the maximum speed of the vehicle in the layout, and $\alpha_{n,m}$ $(0\leq\alpha_{n,m}\leq 1)$ is a random variable with a uniform distribution. Evaluation using other distributions for $\alpha_{n,m}$ is not precluded. The terms $\bar{\boldsymbol{\nu}}_{rx}$ and $\bar{\boldsymbol{\nu}}_{tx}$ are presented respectively by the following equations:

$$\bar{\boldsymbol{\nu}}_{rx}=\boldsymbol{\nu}_{rx}\begin{bmatrix}\sin\theta_{\nu,rx}\cos\phi_{\nu,rx}\\ \sin\theta_{\nu,rx}\sin\phi_{\nu,rx}\\ \cos\theta_{\nu,rx}\end{bmatrix}, \tag{4}$$

$$\bar{\boldsymbol{\nu}}_{tx}=\boldsymbol{\nu}_{tx}\begin{bmatrix}\sin\theta_{\nu,tx}\cos\phi_{\nu,tx}\\ \sin\theta_{\nu,tx}\sin\phi_{\nu,tx}\\ \cos\theta_{\nu,tx}\end{bmatrix}. \tag{5}$$

The remaining parameters were defined in 3GPP TR 38.901 (3GPP, 2018). Regarding the absolute time of arrival, two candidate models were suggested in 3GPP (Ericsson, 2019a). These two models are consistent in the LoS case, and the absolute time is calculated from the propagation distance of the direct path:

$$\bar{\tau}_{\mathrm{LoS}}=\frac{d}{c}, \tag{6}$$

where $d$ is the distance between transmitter and receiver, and $c$ is the velocity of light.

In the NLoS case, however, there are two available candidate models:

$$\bar{\tau}_{\mathrm{NLoS}}=\frac{d}{c}+\Delta\tau. \tag{7}$$

In the first model, the additional part $\Delta\tau$ is stochastically generated according to some distributions (Ericsson, 2019a). The second model is defined according to the distributions of the angle of departure (AoD) and the angle of arrival (AoA) and uses the single-bounce propagation path. However, in the real propagation environment, both single- and multiple-bounce propagation paths exist. Thus, the second model may have conflicts with the real environment. A summary of the above channel measurements is shown in Table 3.

### 3.3 SAGIN channel measurements and models

A large number of channel measurements have been conducted for the SAGIN. All of them focus

**Table 3 Important channel measurement studies for IIoT**

| Reference | Frequency (GHz) | Scenario | Channel characteristics |
|---|---|---|---|
| Rappaport and McGillem (1987) | 1.1–1.5 | Multistory facility and single-story facility | RMS DS and attenuation |
| Miaoudakis et al. (2005) | 2.4 | Manufacturing factory | Attenuation, average delay, RMS DS, and coherence bandwidth |
| Karedal et al. (2007) | 3.1–10.6 | Incinerator hall and MAX-Lab | Power delay profile (PDP), RMS DS, and multipath number |
| Tanghe et al. (2008) | 0.9, 2.4, 5.2 | Wood processing factory and metal processing factory | Path loss, shadow fading, and $K$-factor |
| Luo et al. (2011) | 2.4, 5.8 | Industrial testbed | Path loss and RMS DS |
| Ferrer-Coll et al. (2012) | 0.433, 1.88, 2.45 | High reflective factory and paper warehouse | PDP and path loss |
| Ai et al. (2015) | 0.9, 1.6, 2.45 | Assembly, electronics, and mechanical rooms | Path loss, shadow fading, and channel capacity |
| Holfeld et al. (2016) | 5.85 | Industrial robots | PDP, path loss, and shadow fading |
| Solomitckii et al. (2018) | 28, 60 | Light industry and heavy industry | Path loss and LoS probability |
| Raimundo et al. (2018) | 54, 70 | Factory, computer foyer, office, and corridor | Angular spread, RMS DS, cross-polarization, and path loss |
| Hanssens et al. (2018) | 1.35 | Warehouse | MPCs and cross-polarization |
| Liu L et al. (2018) | 1.1, 1.6, 3.5, 5.8 | Automobile factory | Path loss, $K$-factor, and RMS DS |

on either one network segment, e.g., space, air, and ground, or integration of two of the three network segments. Research on characteristics of land-mobile satellite channels was carried out early in about the 1970s. A series of propagation measurements were conducted in European areas with satellite elevation look angles ranging from 13° to 43° at 1.54 GHz (L-band) (Lutz et al., 1991). Furthermore, based on an extensive statistical evaluation, an analog channel model was developed, which is largely characterized by the time-share of shadowing and the $K$-factor. In an early study (Hess, 1980), excess path loss measurements for land-mobile satellite channels at the ultra-high-frequency (UHF) band of 800 MHz were presented. Measurement results showed that excess path loss on the order of 25 dB is typical in urban situations, while it decreases to under 10 dB in suburban or rural areas.

Apart from the path loss, shadow fading has important effects on the received signals. Single trees were found to attenuate between 10 and 20 dB, with an average median attenuation of 12 dB (Vogel and Goldhirsh, 1986; Goldhirsh and Vogel, 1987). Furthermore, analysis of the results demonstrated that tree shadowing is the deciding factor to dictate fade margin for land-mobile satellite systems, as compared to fades caused by multipath (Vogel and Goldhirsh, 1988). In Vogel and Goldhirsh (1993), static tree attenuation measurements at 20 GHz ($K$-band) on a 30° slant path through a mature Pecan tree with and without leaves showed that median fades exceed about 23 dB and 7 dB, respectively. This indicates that as the frequency increases, the attenuation caused by foliage also increases and becomes significant at the $K$-band.

On the basis of measurement results, some statistical channel models were proposed (Lutz et al., 1991; Loo, 1996; Xie and Fang, 2000; Li WZ et al., 2001). Generally, the channel model can be expressed as the sum of a log-normally distributed random phasor and a Rayleigh phasor:

$$r = z\mathrm{e}^{\mathrm{j}\phi_0} + w\mathrm{e}^{\mathrm{j}\phi}, \tag{8}$$

where $r$ is the received signal, $z\mathrm{e}^{\mathrm{j}\phi_0}$ represents the LoS component, $w\mathrm{e}^{\mathrm{j}\phi}$ represents other multipaths, the phases $\phi_0$ and $\phi$ are uniformly distributed between 0 and $2\pi$, $z$ is log-normally distributed, and $w$ has a Rayleigh distribution. Details about this model can be found in Lutz et al. (1991). In Li WZ et al. (2001), a statistical channel model taking into account weather impairments was proposed. In this case, the probability density function (PDF) of the signal amplitude is

$$p_T(r) = p_\beta(r)p_w(r), \tag{9}$$

where $p_\beta(r)$ and $p_w(r)$ are the PDFs of the mobile fading and weather impairments, respectively. Based on experimental measurements conducted in a tropical area, a tropical weather-aware land-mobile satellite channel model was proposed in Al-Saegh et al. (2017). This model supports diverse atmospheric phenomena, such as rain, clouds, and tropospheric scintillation. Apart from the environment type and the elevation of the satellite, the azimuth angle relative to the driving direction of the mobile terminal was found to affect the channel statistics in Rieche et al. (2015). Furthermore, a statistical land mobile satellite channel model for arbitrary elevation and azimuth angles was proposed via an image-based state estimation method.

The forementioned channel measurements for land-mobile satellites were all conducted using a single antenna at both the transmitter side and the receiver side. Recently, channel measurements using multiple antennas were carried out to investigate the applicability of multiple-antenna techniques in satellite communication systems. In Arndt et al. (2011), a measurement campaign was conducted along the east coast of the United States. Four antennas were used at the receiver side to record the power levels. It was found that selection combining would require at least four antennas to achieve the same performance as that of two-antenna maximal-ratio combining. Furthermore, the corresponding antenna diversity gain of each antenna configuration is independent of the environment. In Lacoste et al. (2010), experimental propagation results derived from multiple-input-single-output (MISO) and single-input-multiple-output (SIMO) land-mobile satellite measurements were presented. Analysis indicates that spatial diversity at the receiver side can significantly reduce the fading margin. In Lacoste et al. (2012), MIMO configurations were used in channel measurements. Furthermore, dual-circular polarization antennas were used to receive the signals. Through analysis of channel capacity statistics, it was found in Fig. 13 that the MIMO approach brings a significant capacity gain as

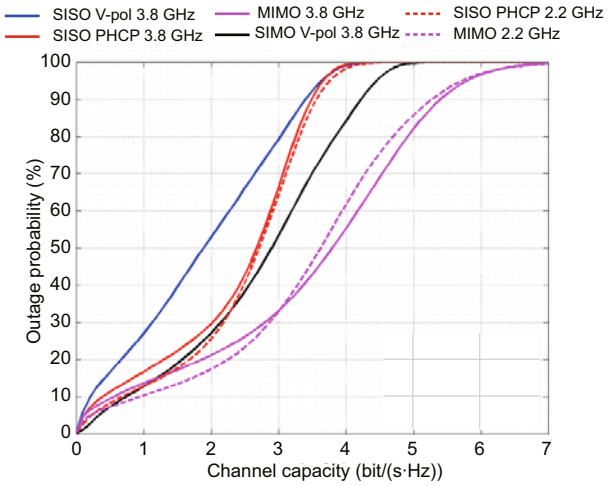


**Fig. 13 SISO, SIMO, and MIMO channel capacities (SNR=10 dB)**

Reprinted from Lacoste et al. (2010), Copyright 2010, with permission from IEEE

compared to single-input-single-output (SISO) systems, but for low outage probabilities (less than 15%), they have similar performances. In Nikolaidis et al. (2016), dual-polarized MIMO channel measurements were presented, which were conducted in a land mobile satellite pedestrian scenario. The extracted results showed that the ergodic capacity of the dual-polarized MIMO channel is 4.3 and 4.1 bits/(s·Hz) for LoS and NLoS propagation conditions, respectively. More reviews of channel measurements for land-mobile satellite communication systems can be found in Petropoulou et al. (2014).

For air-to-ground communications, a number of channel measurement campaigns have been carried out to understand the channel characteristics, such as path loss, shadowing, DS, and Doppler spread (Khawaja et al., 2019). In Matolak and Sun (2017a, 2017b) and Sun and Matolak (2017), a series of channel measurements for most of the typical ground site-local environments, e.g., over water, hilly/mountainous, suburban, and near-urban, were presented. Based on the measurement results, the path loss is described by a log-distance model with small corrections for flight direction. The log-distance model is given by

$$\mathrm{PL}(d) = A_0 + 10n\log(d/d_{\min}) + X + \zeta F_A, \quad (10)$$

where $d_{\min} \le d \le d_{\max}$, $A_0$ is a constant at the minimum valid link distance of $d_{\min}$, $d_{\max}$ is the maximum valid link distance, $n$ is the path loss exponent, $\zeta = -1$ indicates that the aerial vehicle travels toward the ground station and $\zeta = +1$ is its opposite, $F_A$ is the small adjustment factor for the direction of travel, and $X$ is a zero-mean Gaussian random variable with the standard derivation $\sigma_X$. This log-distance model is similar to the CI path loss model (Samimi et al., 2015) for terrestrial propagation channels but considers the flight direction effect, which is helpful for aerial applications. More path loss estimates using log-distance models can be found in Feng et al. (2006), Simunek et al. (2011), Yanmaz et al. (2011), Al-Hourani et al. (2014), and Ono et al. (2015).

Delay dispersion is also an important channel property for air-to-ground communication systems, which can incur inter-symbol interference. In Khawaja et al. (2016), the mean excess delay and RMS DS results for open and sub-urban areas were presented based on experimental measurements. In Matolak and Sun (2017a), it was found that DS in the over-water channels is dominated by the LoS path and the reflected path from the water surface. Thus, the extracted DSs are typically small, about 10 ns. In a hilly terrain suburban environment, major values of DSs are within the range of 10–20 ns, but a larger value of nearly 1000 ns also occasionally occurs (Sun and Matolak, 2017). Due to the motion of scatterers and transceivers, multipaths are received with different Doppler frequencies, which produces spectral broadening. In Willink et al. (2015), the Doppler effects were analyzed based on air-to-ground channel measurements at 915 MHz. The maximum Doppler shift of 100 MHz occurs when the UAV is moving directly away from the land station. However, Doppler spread results extracted from air-to-ground channel measurements are scarce. Simulations are often used to find the Doppler shift (Haas, 2002; Tu and Shimamoto, 2009). In air-to-ground communications, there is a higher likelihood of LoS propagation. In the case where a LoS component exists, small-scale fading follows a Rice distribution. In Matolak and Sun (2014, 2017b), Matolak (2015), and Sun and Matolak (2017), the $K$-factor was measured from urban, suburban, hilly and mountainous settings, and water and sea scenarios. The mean value of the $K$-factor varies in different scenarios and bands. For example, the mean values of the $K$-factor for urban areas were 12 dB and 27.4 dB for the L-band and C-band, respectively (Matolak and Sun, 2017b). Furthermore, it was found that the $K$-factor is proportional to the

elevation angle (Newhall et al., 2003) and is a function of the link distance (Tu and Shimamoto, 2009). In terms of the angle dispersion, though some air-to-ground channel measurements have been conducted with MIMO antenna configurations (Newhall et al., 2003; Zhang C and Hui, 2011; Gao et al., 2013; Willink et al., 2015), analysis of angle dispersion is scarce. In Wentz and Stojanovic (2015) and Cheng X and Li (2019), MIMO radio channel models for air-to-ground communication systems were proposed, but they are deterministic models, rather than stochastic models based on channel measurements.

A number of channel measurements for terrestrial communication systems have been carried out (Matolak et al., 2005; Luan et al., 2013; Martínez et al., 2014; Chen XB et al., 2016; Zhang JH et al., 2017b, 2018; Tang et al., 2018; Wang CX et al., 2018). In Goddemeier and Wietfeld (2015), air-to-air channel characteristics were investigated by extending the Rice channel model. However, channel measurements for air-to-air communication systems are still scarce. Specifically, for space-to-space communication systems (Huang C et al., 2016), according to our knowledge, there is no dedicated channel measurement yet. A summary of the above channel measurements for SAGIN is given in Table 4.

### 3.4 Machine learning in channel modeling

Channel models can be categorized as the deterministic model, geometry-based stochastic model (GBSM), and non-geometric stochastic model. The deterministic channel model, similar to the ray-tracing based model, characterizes the propagation parameters in a computable deterministic manner. The ray-tracing approach models the radio channel according to the electromagnetic field theory and the theoretic propagation principles based on the electromagnetic and geometry information of the reconstructed environment. In GBSM, the scatterers in the environment are abstracted as randomly distributed clusters, and each cluster is composed of several paths. GBSM takes advantage

**Table 4 Important channel measurement studies for the space-air-ground integrated network**

| Reference | Category | Frequency (GHz) | Antenna configuration | Channel characteristics |
|---|---|---|---|---|
| Hess (1980) | Space-to-ground | 0.86, 1.55 | SISO | Path loss |
| Goldhirsh and Vogel (1987) | Space-to-ground | 0.87 | SISO | Tree shadowing |
| Vogel and Goldhirsh (1988) | Space-to-ground | 1.5, 0.87 | SISO | Tree shadowing |
| Lacoste et al. (2010) | Space-to-ground | 2.2 | SIMO and MISO | Fade levels |
| Arndt et al. (2011) | Space-to-ground | 2.19 | SIMO | Capacity |
| Lacoste et al. (2012) | Space-to-ground | 2.2, 3.8 | SIMO and MIMO | Fade levels, $K$-factor, capacity, and cross-polarization discrimination |
| Nikolaidis et al. (2016) | Space-to-ground | 2 | MIMO | Fade levels, shadowing, coherence distance, capacity, and power spectrum |
| Al-Saegh et al. (2017) | Space-to-ground | 12, 14, 16 | SISO | Fade levels, shadowing, and $K$-factor |
| Newhall et al. (2003) | Air-to-ground | 2.05 | SIMO | Path loss, DS, excess delay, and $K$-factor |
| Ono et al. (2015) | Air-to-ground | 2.3 | SISO | Path loss |
| Willink et al. (2015) | Air-to-ground | 0.92 | MIMO | Path loss, DS, Doppler shift, and spatial correlation |
| Matolak and Sun (2017a) | Air-to-ground | 0.97, 5 | SISO | Path loss, $K$-factor, DS, and spatial correlation |
| Khawaja et al. (2016) | Air-to-ground | 4.3 | SISO | Path loss, shadowing, excess delay, and DS |
| Luan et al. (2013) | Ground-to-ground | 2.4 | SISO | Path loss, shadowing, and $K$-factor |
| Martínez et al. (2014) | Ground-to-ground | 5.8 | Massive MIMO | Path power, correlation property, eigenvalue, and condition number |
| Chen XB et al. (2016) | Ground-to-ground | 28 | SISO | Human-body shadowing |
| Goddemeier and Wietfeld (2015) | Air-to-air | 2.4 | SISO | Fade levels and $K$-factor |

of environment-specific and stochastic modeling. In contrast, the non-geometric stochastic model describes and determines physical parameters in a completely stochastic way by prescribing the underlying probability distribution functions without assuming an underlying geometry.

These channel models are often optimized for mathematically simplified models (linear, stationary, and Gaussian distribution). However, differences between these models and the real channel exist due to the imperfect assumption conditions. ML does not require a rigidly defined model for representation and could be optimized in an end-to-end manner for a real system with harsh realistic effects (O'Shea and Hoydis, 2017). Moreover, with the wide frequency range, huge bandwidth, large number of antennas, and versatile scenarios brought in by B5G, the volume of channel measurement data will be quite large. Processing of measurement data is usually a time-consuming process and requires great computational power (Zhang J, 2016). Thus, it is reasonable to develop channel models by taking advantage of data mining and ML algorithms.

Recently, a variety of attempts have been made to apply big data analytics such as ML to wireless channel modeling. Considering the significance of parameters in channel modeling, some researchers focus on predicting channel parameters using ML methods which enhance the prediction accuracy and reduce the complexity. In Li W et al. (2019), a back propagation (BP) neural network was used to model the large-scale fading. In addition, an Elman neural network was used to predict the channel impulse response (CIR). Yang et al. (2019) proposed prediction methods for path loss and DS in air-to-ground mm-wave channels based on ML. In Dai et al. (2018), ML algorithms were used to predict received signal strengths at the user side. The numerical results showed that the support vector machine (SVM) outperforms other classifiers in terms of prediction accuracy. In Huang HJ et al. (2018), a deep neural network (DNN) was employed to conduct offline and online learning to achieve super-resolution AoA estimation and channel estimation in the massive MIMO system. In Navabi et al. (2018), neural networks were also applied to predict channel features that are not directly observable in BS, such as AoD of the dominant propagation paths in the user channels. In Lu et al. (2018), a convolutional neural network (CNN) was applied to predict channel characteristics for 3D mm-wave massive MIMO indoor channels. With the location information of the transmitter and the receiver, which is input in CNN, the channel statistical characteristics of the sub-channels in a specified indoor scenario can be predicted.

GBSM is a clustered structure model, where MPCs are grouped into clusters. Moreover, the cluster statistics are characterized for parameters such as the number of MPCs, positions of scatterers, delay, and angular spreads. Thus, a clustering algorithm can improve the model precision. In Li YP et al. (2018), the Gaussian mixture model (GMM) was introduced to implement channel multipath clustering, and the similarity of MPCs could be revealed. Then, the variational Bayesian (VB) algorithm was used to optimize the GMM parameters to enhance the searching ability and further to determine the optimal number of Gaussian distributions without resorting to cross-validation.

Zhang J (2016) proposed a cluster-nuclei-based channel model based on big data theories, which takes advantage of both the stochastic model and the deterministic model. Cluster-nuclei are defined as clusters with a certain shape, which dominate the generation in various scenarios and have a relationship with scatterers in the propagation environment. First, computer vision and image processing are introduced to identify the texture from the picture of measurement scenarios and reconstruct the 3D wireless propagation environment. Meanwhile, the channel parameters are extracted from the measurement data by channel parameter estimation algorithms. Then, MPCs are clustered with the clustering algorithms, such as $K$-means and GMM. Next, the key step is to research the mapping relationship between scatterers from the propagation environment and the clusters obtained from the channel measurements, so as to obtain the mechanism of the cluster-nuclei (Fig. 14). Finally, with the limited number of cluster-nuclei, CIR can be produced using ML methods. In Ma et al. (2017), a channel modeling method was proposed based on the principal component analysis (PCA) method, which has better accuracy than the standardized GBSM. The hidden features and structures extracted from the measured channel data are used to reconstruct CIR. In Li HH et al. (2017), a tomographic channel model was proposed, in which GMM is applied to acquire the

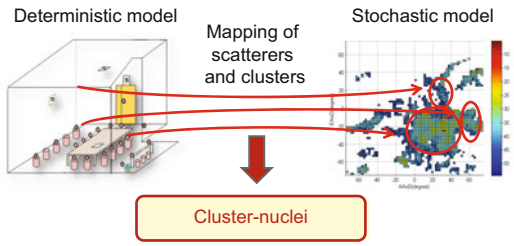


**Fig. 14 Mechanism of cluster-nuclei**

distribution of the wireless channel parameters, and CNN is applied to automatically distinguish between the different wireless channels.

The purpose of using ML algorithms in wireless channel modeling is that many problems can resort to classification, clustering, and regression algorithms. By learning and training the big data sets in channel measurements, the channel models can become more intelligent to achieve better performance and adapt to various scenarios. In Table 5, we summarize the aforementioned applications and studies on ML algorithms in wireless channel modeling.

## 4 Future outlook for 6G channel measurements and models

Until now, much effort has been given to characterize the channel for 6G. However, there are some open issues before completing 6G channel measurements and modeling. In the following, we discuss the outlook for 6G channel measurements and models in terms of the above-mentioned four aspects.

### 4.1 THz channel measurements and models

THz channel characterization, as a fundamental issue, is quite essential, and several challenging issues need to be addressed in the future. First, a reliable THz channel sounding technique is the guarantee to obtain first-hand accurate channel data. As mentioned in the previous section, none of the present channel sounding systems meet the full requirements of all the channel properties. Apart from studying new sounding techniques, the reliability and calibration of the presently available sounding systems also need to be investigated. Second, extensive THz channel measurement campaigns are encouraged for investigating not only the propagation mechanism but also the basic channel parameters, such as path loss, delay, and angle in various scenarios. Specifically, knowledge of the spatial characteristics of the THz channel is relatively deficient in current research. Third, with the large-scale order of frequency, bandwidth, and MIMO in the THz band, the non-stationary THz channel characteristics cannot be neglected. For example, when the bandwidth becomes extremely wide compared with the center frequency, the channel will be non-stationary over the whole bandwidth. Moreover, other potential effects on the THz band, such as molecular absorption and blockage, need to be considered. Finally, a complete, accurate, and flexible THz channel model is the most essential issue. The ray-tracing method is the most studied one for the THz channel in the literature. However, both deterministic and stochastic channel modeling methods have their pros and cons. It is still an open issue to choose either method or

**Table 5 Applications of machine learning in wireless channel modeling**

| Reference | Task | Algorithm | Application(s) |
|---|---|---|---|
| Dai et al. (2018) | Parameter prediction | SVM | Prediction of strength of the received signal |
| Huang HJ et al. (2018) | Parameter prediction | DNN | AoA estimation and channel estimation |
| Navabi et al. (2018) | Parameter prediction | CNN | AoD prediction |
| Lu et al. (2018) | Parameter prediction | CNN | Prediction of channel characteristics |
| Yang et al. (2019) | Parameter prediction | Random forest and KNN | Path loss and DS prediction |
| Li YP et al. (2018) | Clustering | VB-GMM | Channel multipath clustering |
| Zhang J (2016) | Modeling | ANN | Production of the CIR with a limited number of cluster-nuclei |
| Ma et al. (2017) | Modeling | PCA | Reconstruction of CIR by extraction of channel features |
| Li HH et al. (2017) | Modeling | GMM and CNN | Extraction of channel features and identification of different wireless channels |

SVM: support vector machine; DNN: deep neural network; CNN: convolutional neural network; KNN: $k$ nearest neighbor; VB-GMM: variational Bayesian Gaussian mixture model; ANN: artificial neural network; PCA: principal component analysis

look for a new mixed method for the THz channel model.

### 4.2 IIoT channel measurements and models

Although some special properties, such as dual mobility and absolute time of arrival, have been added in the present wireless channel model, basically, it is still not enough. The correlation property of the wireless channels just inherits the indoor office parameters. Besides, the blockage model in the IIoT scenario still adopts the blockage model B in the standard (3GPP, 2018). However, for factories with massive connections, the sensor devices are quite similar, and they are usually embedded in larger devices. Their correlation property and the blockage model may be further studied. There are many noise sources in the factory, such as motors, heavy machinery, inverters, voltage regulators, welding equipment, and electric switch contacts. Therefore, modeling interference and noise is another considerable problem when designing a robust wireless network in industrial applications.

### 4.3 SAGIN channel measurements and models

Currently, a number of channel measurements have been conducted to research the channel characteristics for terrestrial, space-to-ground, and air-to-ground communication systems. Some statistical channel models and deterministic channel models have been proposed to describe the channels. However, more channel measurements for air-to-air, space-to-space, and space-to-air communication systems are needed to deeply understand the channel properties. Moreover, a unified channel model is needed to design the space-air-ground communication systems, rather than several channel models for different scenarios. Furthermore, some key technologies in 5G, e.g., massive MIMO and mm-wave, may be considered in SAGIN. These technologies can help improve the capacity of the integrated network. Correspondingly, channel measurements should be conducted to evaluate the performance of these technologies in SAGIN.

### 4.4 Machine learning in channel modeling

Considering that the channel measurement data of 5G already appear in big volumes because of the increased number of antennas, huge bandwidth, and versatile application scenarios, stochastic channel models such as GBSM lack physical meaning, and deterministic channel models such as the ray-tracing methods are highly complex and rely on the precision of the geographic information. The future intelligent channel modeling methodology for B5G and 6G should take advantage of both stochastic and deterministic models, aiming to predict and model the channel more precisely and efficiently. Thus, supporting future wireless research, especially on the massive MIMO, mm-wave, and versatile scenarios, is important for the development of future communication.

Based on ML methods, the intelligent channel model can learn channel characteristics and hidden rules from the channel database. Hence, channel fading will be predicted automatically. Fig. 15 shows a specific wireless propagation environment, and Fig. 16 shows the channel fading prediction by intelligent channel modeling based on big data and ML. According to the mapping relation between the environment and cluster-nuclei, cluster-nuclei can be extracted from the map information. Correspondingly, the radio propagation can be reproduced. For the proposed ML-based channel modeling methodology, some open issues still need to be researched in the future work. First, a trusted channel database is needed. Although different universities

**Fig. 15 Wireless propagation environment**

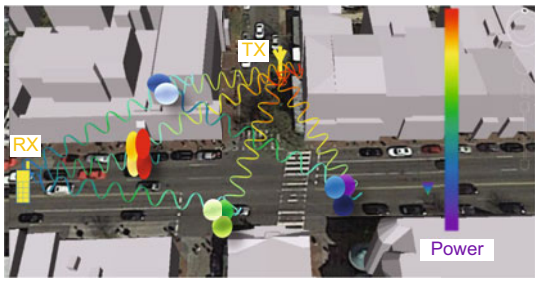


**Fig. 16 Channel fading predicted by intelligent channel modeling**

and companies have their data collected by their platforms, such data are labeled with different frequencies, bandwidths, antenna configurations, and scenarios. Such data forms need to be evaluated, and the data need to be merged into the database. Second, methods for mapping clusters with scatterers and describing the physical meaning of cluster-nuclei are needed. Third, many ML algorithms have been proposed, but which one is more effective in generating the channel model from cluster-nuclei is not clear. Generally, more effort is required to overcome the challenges and achieve intelligent channel modeling.

## 5 Conclusions

This paper introduces several promising technologies and applications for 6G, including THz communication, IIoT, SAGIN, and ML. Based on the analysis of these technologies and applications, 6G channel models are expected to support higher frequency and larger bandwidth, ultra-large-scale antenna arrays, and diverse application scenarios. Furthermore, this paper provides a review of channel measurements and models in terms of these technologies and applications. Specific channel properties and modeling methods are discussed. For example, in terms of the THz channel, the dependency of channel parameters on the frequency needs to be considered in models due to the large range of frequencies. IIoT communication scenarios are rich-scattering because there are many metal objects, which makes channel models for traditional cell communications unable to correctly describe the channel properties, e.g., RMS DS and the LoS probability. The difference in the communication distance is large between the space-to-ground channel and air-to-ground channel. Thus, space-to-ground channel models think more of large-scale fading caused by the atmosphere. ML can help extract the hidden features and structures in modeling channels by taking advantage of both stochastic models and deterministic models. Finally, the outlook for channel measurements and models for 6G is discussed. As yet, research on channel measurements and modeling is in its infancy, and further efforts are needed to support the design of 6G communication systems.

### Contributors

Jian-hua ZHANG designed the research, and revised and edited the final version. Pan TANG leaded the drafting of the manuscript. Li YU, Tao JIANG, and Lei TIAN helped draft the manuscript.

### Compliance with ethics guidelines

Jian-hua ZHANG, Pan TANG, Li YU, Tao JIANG, and Lei TIAN declare that they have no conflict of interest.

### References

3GPP, 2018. Study on Channel Model for Frequencies from 0.5 to 100 GHz. Technical Report TR 38.901, 3GPP.

3GPP, 2019. Study on Evaluation Methodology of New Vehicle-to-Everything (V2X) Use Cases for LTE and NR. Technical Report TR 37.885, 3GPP.

5G-ACIA, 2018. LS on Channel Model for Indoor Industrial Scenarios. Proposal RP-181521, 5G-ACIA.

Ai Y, Cheffena M, Li Q, 2015. Radio frequency measurements and capacity analysis for industrial indoor environments. Proc 9th European Conf on Antennas and Propagation, p.1-5.

Ali E, Ismail M, Nordin R, et al., 2017. Beamforming techniques for massive MIMO systems in 5G: overview, classification, and trends for future research. *Front Inform Technol Electron Eng*, 18(6):753-772. https://doi.org/10.1631/FITEE.1601817

Almeida JJH, Lopes PB, Akamine C, et al., 2018. An application of neural networks to channel estimation of the ISDB-TB FBMC system. https://arxiv.org/abs/1803.01141

Alpaydin E, 2006. Introduction to Machine Learning. MIT Press, USA.

Al-Hourani A, Kandeepan S, Jamalipour A, 2014. Modeling air-to-ground path loss for low altitude platforms in urban environments. IEEE Global Communications Conf, p.2898-2904. https://doi.org/10.1109/GLOCOM.2014.7037248

Al-Saegh AM, Sali A, Mandeep JS, et al., 2017. Channel measurements, characterization, and modeling for land mobile satellite terminals in tropical regions at Ku-band. *IEEE Trans Veh Technol*, 66(2):897-911. https://doi.org/10.1109/TVT.2016.2563038

Arndt D, Ihlow A, Heuberger A, et al., 2011. Antenna diversity for mobile satellite applications: performance evaluation based on measurements. Proc 5th European Conf on Antennas and Propagation, p.3729-3733.

Baum LE, Petrie T, 1966. Statistical inference for probabilistic functions of finite state Markov chains. *Ann Math Stat*, 37(6):1554-1563.

Berardinelli G, Mahmood NH, Rodriguez I, et al., 2018. Beyond 5G wireless IRT for Industry 4.0: design principles and spectrum aspects. IEEE Globecom Workshops, p.1-6. https://doi.org/10.1109/glocomw.2018.8644245

Bishop CM, 2006. Pattern Recognition and Machine Learning. Springer, New York.

Cerwall P, Jonsson P, Möller R, et al., 2015. Ericsson Mobility Report. Telefonaktiebolaget LM Ericsson, Stockholm, Sweden.

Chen JJ, Yin XF, Cai XS, et al., 2017. Measurement-based massive MIMO channel modeling for outdoor LoS and NLoS environments. *IEEE Access*, 5:2126-2140. https://doi.org/10.1109/ACCESS.2017.2652983

Chen XB, Tian L, Tang P, et al., 2016. Modelling of human body shadowing based on 28 GHz indoor measurement results. IEEE 84th Vehicular Technology Conf, p.1-5. https://doi.org/10.1109/VTCFall.2016.7881093

Chen XF, Han Z, Zhang HG, et al., 2018. Wireless resource scheduling in virtualized radio access networks using stochastic learning. *IEEE Trans Mob Comput*, 17(4):961-974. https://doi.org/10.1109/TMC.2017.2742949

Cheng CL, Kim S, Zajić A, 2017. Comparison of path loss models for indoor 30 GHz, 140 GHz, and 300 GHz channels. Proc 11th European Conf on Antennas and Propagation, p.716-720. https://doi.org/10.23919/EuCAP.2017.7928124

Cheng X, Li YR, 2019. A 3-D geometry-based stochastic model for UAV-MIMO wideband nonstationary channels. *IEEE Int Things J*, 6(2):1654-1662. https://doi.org/10.1109/JIOT.2018.2874816

Cisco, 2019. Cisco Visual Networking Index: Global Mobile Data Traffic Forecast Update, 2017-2022 White Paper. Cisco Systems, Inc., CA, USA.

CMCC, BUPT, 2018a. New Measurements and Modelling on Fast Fading in IIOT Scenarios. Proposal RP-1904743, 3GPP.

CMCC, BUPT, 2018b. New Measurements and Modelling on Pathloss in IIOT Scenarios. Proposal RP-1904742, 3GPP.

CMRI, 2019. The Outlook and Demand Report for 2030+. China Mobile Resesrch Institute, Bejing (in Chinese). https://cmri.chinamobile.com/news/5985.html [Accessed on Jan. 4, 2020].

Cortes C, Vapnik V, 1995. Support-vector networks. *Mach Learn*, 20(3):273-297.

Dahlman E, Mildh G, Parkvall S, et al., 2014. 5G wireless access: requirements and realization. *IEEE Commun Mag*, 52(12):42-47. https://doi.org/10.1109/MCOM.2014.6979985

Dai L, Zhang H, Zhuang Y, 2018. Propagation-model-free coverage evaluation via machine learning for future 5G networks. IEEE 29th Annual Int Symp on Personal, Indoor and Mobile Radio Communications, p.1-5. https://doi.org/10.1109/PIMRC.2018.8580992

Darak SJ, Zhang HG, Palicot J, et al., 2017. Decision making policy for RF energy harvesting enabled cognitive radios in decentralized wireless networks. *Dig Signal Process*, 60:33-45. https://doi.org/10.1016/j.dsp.2016.08.014

Dreyfus SE, 2012. Artificial neural networks, back propagation, and the Kelley-Bryson gradient procedure. *J Guid Contr Dynam*, 13(5):926-928.

Ericsson, 2019a. Summary of Email Discussion on Additional Modelling Components. Proposal RP-1905197, 3GPP.

Ericsson, 2019b. Views on Additional Modelling Components. Proposal RP-1905203, 3GPP.

Feng QX, McGeehan J, Tameh EK, et al., 2006. Path loss models for air-to-ground radio channels in urban environments. IEEE 63rd Vehicular Technology Conf, p.2901-2905. https://doi.org/10.1109/VETECS.2006.1683399

Ferrer-Coll J, Ängskog P, Chilo J, et al., 2012. Characterisation of highly absorbent and highly reflective radio wave propagation environments in industrial applications. *IET Commun*, 6(15):2404-2412. https://doi.org/10.1049/iet-com.2012.0028

Freund Y, Schapire R, Abe N, 1999. A short introduction to boosting. *J Jpn Soc Artif Intell*, 14(5):771-780.

Gao X, Chen Z, Hu Y, 2013. Analysis of unmanned aerial vehicle MIMO channel capacity based on aircraft attitude. *WSEAS Trans Inform Sci Appl*, 10(2):58-67.

Giordani M, Polese M, Mezzavilla M, et al., 2019. Towards 6G networks: use cases and technologies. https://arxiv.org/abs/1903.12216

Goddemeier N, Wietfeld C, 2015. Investigation of air-to-air channel characteristics and a UAV specific extension to the rice model. IEEE Globecom Workshops, p.1-5. https://doi.org/10.1109/GLOCOMW.2015.7414180

Goldhirsh J, Vogel W, 1987. Roadside tree attenuation measurements at UHF for land mobile satellite systems. *IEEE Trans Antenn Propag*, 35(5):589-596. https://doi.org/10.1109/TAP.1987.1144137

Goldsmith A, Jafar SA, Jindal N, et al., 2003. Capacity limits of MIMO channels. *IEEE J Sel Areas Commun*, 21(5):684-702. https://doi.org/10.1109/JSAC.2003.810294

Haas E, 2002. Aeronautical channel modeling. *IEEE Trans Veh Technol*, 51(2):254-264. https://doi.org/10.1109/25.994803

Hanssens B, Kshetri SR, Tanghe E, et al., 2018. Measurement-based analysis of dense multipath components in a large industrial warehouse. 12th European Conf on Antennas and Propagation, p.1-5. https://doi.org/10.1049/cp.2018.0453

Hess GC, 1980. Land-mobile satellite excess path loss measurements. *IEEE Trans Veh Technol*, 29(2):290-297. https://doi.org/10.1109/T-VT.1980.23854

Hochreiter S, Schmidhuber J, 1997. Long short-term memory. *Neur Comput*, 9(7):1735-1780.

Holfeld B, Wieruch D, Raschkowski L, et al., 2016. Radio channel characterization at 5.85 GHz for wireless M2M communication of industrial robots. IEEE Wireless Communications and Networking Conf, p.1-7. https://doi.org/10.1109/WCNC.2016.7564890

Hu BB, Nuss MC, 1995. Imaging with terahertz waves. *Opt Lett*, 20(16):1716-1718. https://doi.org/10.1364/OL.20.001716

Huang C, Huang KW, Wen Y, et al., 2016. A propose of the ISS space-to-space communication system by multiplexing ground mobile communication frequency resources. 6th Int Conf on Instrumentation & Measurement, Computer, Communication and Control, p.567-569. https://doi.org/10.1109/IMCCC.2016.123

Huang HJ, Yang J, Song Y, et al., 2018. Deep learning for super-resolution channel estimation and DOA estimation based massive MIMO system. *IEEE Trans Veh Technol*, 67(9):8549-8560. https://doi.org/10.1109/TVT.2018.2851783

Huawei, HiSilicon, 2018. Preliminary Channel Measurement on Large-Scale Propagation Loss for Indoor Factory Environment. Proposal RP-1904706, 3GPP.

ITU-R, 2013. Attenuation by Atmospheric Gases. Recommendation P.676-10, ITU-R, Geneva, Switzerland.

ITU-R, 2015. IMT Traffic Estimates for the Years 2020 to 2030. Report M.2370, ITU-R, Geneva, Switzerland.

ITU-T, 2019. Architectural Framework for Machine Learning in Future Networks Including IMT-2020. Recommendation Y.3172, ITU-T, Geneva, Switzerland.

Jacob M, Priebe S, Dickhoff R, et al., 2012. Diffraction in mm and sub-mm wave indoor propagation channels. *IEEE Trans Microw Theory Technol*, 60(3):833-844. https://doi.org/10.1109/TMTT.2011.2178859

Jansen C, Piesiewicz R, Mittleman D, et al., 2008. The impact of reflections from stratified building materials on the wave propagation in future indoor terahertz communication systems. *IEEE Trans Antenn Propag*, 56(5):1413-1419. https://doi.org/10.1109/TAP.2008.922651

Jansen C, Priebe S, Moller C, et al., 2011. Diffuse scattering from rough surfaces in THz communication channels. *IEEE Trans Terahertz Sci Technol*, 1(2):462-472. https://doi.org/10.1109/TTHZ.2011.2153610

Jiang CX, Zhang HJ, Ren Y, et al., 2016. Machine learning paradigms for next-generation wireless networks. *IEEE Wirel Commun*, 24(2):98-105. https://doi.org/10.1109/MWC.2016.1500356WC

Joo EM, Zhou Y, 2009. Theory and Novel Applications of Machine Learning. IntechOpen, London, UK.

Kalman RE, 1960. A new approach to linear filtering and prediction problems. *J Bas Eng*, 82(1):35-45.

Karedal J, Wyne S, Almers P, et al., 2007. A measurement-based statistical model for industrial ultra-wideband channels. *IEEE Trans Wirel Commun*, 6(8):3028-3037. https://doi.org/10.1109/TWC.2007.051050

Khalid N, Akan OB, 2016. Wideband THz communication channel measurements for 5G indoor wireless networks. IEEE Int Conf on Communications. https://doi.org/10.1109/ICC.2016.7511280

Khawaja W, Guvenc I, Matolak D, 2016. UWB channel sounding and modeling for UAV air-to-ground propagation channels. IEEE Global Communications Conf, p.1-7. https://doi.org/10.1109/GLOCOM.2016.7842372

Khawaja W, Guvenc I, Matolak DW, et al., 2019. A survey of air-to-ground propagation channel modeling for unmanned aerial vehicles. *IEEE Commun Surv Tutor*, 21(3):2361-2391. https://doi.org/10.1109/COMST.2019.2915069

Kim S, Zajić AG, 2015. Statistical characterization of 300-GHz propagation on a desktop. *IEEE Trans Veh Technol*, 64(8):3330-3338. https://doi.org/10.1109/TVT.2014.2358191

Lacoste F, Carvalho F, Fontan FP, et al., 2010. MISO and SIMO measurements of the land mobile satellite propagation channel at S-band. Proc 4th European Conf on Antennas and Propagation, p.1-5.

Lacoste F, Lemorton J, Casadebaig L, et al., 2012. Measurements of the land mobile and nomadic satellite channels at 2.2 GHz and 3.8 GHz. 6th European Conf on Antennas and Propagation, p.2422-2426. https://doi.org/10.1109/EuCAP.2012.6206356

Lei MY, Zhang JH, Lei T, et al., 2015. 28-GHz indoor channel measurements and analysis of propagation characteristics. IEEE 25th Annual Int Symp on Personal, Indoor, and Mobile Radio Communication. https://doi.org/10.1109/PIMRC.2014.7136161

Li HH, Li YZ, Zhou SD, et al., 2017. Wireless channel feature extraction via GMM and CNN in the tomographic channel model. *J Commun Inform Netw*, 2(1):41-51. https://doi.org/10.1007/s41650-017-0004-z

Li JZ, Ai B, He RS, et al., 2017. Indoor massive multiple-input multiple-output channel characterization and performance evaluation. *Front Inform Technol Electron Eng*, 18(6):773-787. https://doi.org/10.1631/FITEE.1700021

Li W, Zhang JH, Ma XC, et al., 2019. The way to apply machine learning to IoT driven wireless network from channel perspective. *China Commun*, 16(1):148-164.

Li WZ, Law CL, Dubey VK, et al., 2001. Ka-band land mobile satellite channel model incorporating weather effects. *IEEE Commun Lett*, 5(5):194-196. https://doi.org/10.1109/4234.922757

Li Y, Zhao L, Wang H, 2012. A novel mobility model for clustered MANET. 8th Int Conf on Wireless Communications, Networking and Mobile Computing, p.1-4. https://doi.org/10.1109/WiCOM.2012.6478340

Li YP, Zhang JH, Ma ZY, et al., 2018. Clustering analysis in the wireless propagation channel with a variational Gaussian mixture model. *IEEE Trans Big Data*, online. https://doi.org/10.1109/TBDATA.2018.2840696

Lin L, Zhu M, 2018. Efficient tracking of moving target based on an improved fast differential evolution algorithm. *IEEE Access*, 6:6820-6828. https://doi.org/10.1109/ACCESS.2018.2793298

Liu GY, Hou XY, Wang F, et al., 2016. Achieving 3D-MIMO with massive antennas from theory to practice with evaluation and field trial results. *IEEE Syst J*, 11(1):62-71. https://doi.org/10.1109/JSYST.2015.2477503

Liu JJ, Shi YP, Fadlullah ZM, et al., 2018. Space-air-ground integrated network: a survey. *IEEE Commun Surv Tutor*, 20(4):2714-2741. https://doi.org/10.1109/COMST.2018.2841996

Liu L, Zhang K, Tao C, et al., 2018. Channel measurements and characterizations for automobile factory environments. 20th Int Conf on Advanced Communication Technology, p.234-238. https://doi.org/10.23919/ICACT.2018.8323708

Liu XQ, Chen HH, Chen SY, et al., 2017. Symbol cyclic-shift equalization algorithm—a CP-free OFDM/OFDMA system design. *IEEE Trans Veh Technol*, 66(1):282-294. https://doi.org/10.1109/TVT.2016.2542106

Loo C, 1996. Statistical models for land mobile and fixed satellite communications at Ka band. Proc Vehicular Technology Conf, p.1023-1027. https://doi.org/10.1109/VETEC.1996.501466

Lu B, Wang CX, Jie H, et al., 2018. Predicting wireless mmwave massive MIMO channel characteristics using machine learning algorithms. *Wirel Commun Mob Comput*, 2018:9783863. https://doi.org/10.1155/2018/9783863

Luan FY, Zhang Y, Xiao LM, et al., 2013. Fading characteristics of wireless channel on high-speed railway in hilly terrain scenario. *Int J Antenn Propag*, 2013:378407. https://doi.org/10.1155/2013/378407

Luo SP, Polu N, Chen ZX, et al., 2011. RF channel modeling of a WSN testbed for industrial environment. IEEE Radio and Wireless Symp, p.375-378. https://doi.org/10.1109/RWS.2011.5725435

Lutz E, Cygan D, Dippold M, et al., 1991. The land mobile satellite communication channel-recording, statistics, and channel model. *IEEE Trans Veh Technol*, 40(2):375-386. https://doi.org/10.1109/25.289418

Ma XC, Zhang JH, Zhang YX, et al., 2017. A PCA-based modeling method for wireless MIMO channel. IEEE Conf on Computer Communications Workshops, p.874-879. https://doi.org/10.1109/infcomw.2017.8116491

Martínez ÀO, de Carvalho E, Nielsen JØ, 2014. Towards very large aperture massive MIMO: a measurement based study. IEEE Globecom Workshops, p.281-286. https://doi.org/10.1109/GLOCOMW.2014.7063445

Marzetta TL, 2010. Noncooperative cellular wireless with unlimited numbers of base station antennas. *IEEE Trans Wirel Commun*, 9(11):3590-3600. https://doi.org/10.1109/TWC.2010.092810.091092

Matolak DW, 2015. Channel characterization for unmanned aircraft systems. 9th European Conf on Antennas and Propagation, p.1-5.

Matolak DW, Sun RY, 2014. Antenna and frequency diversity in the unmanned aircraft systems bands for the over-sea setting. IEEE/AIAA 33rd Digital Avionics Systems Conf, p.1-10. https://doi.org/10.1109/DASC.2014.6979495

Matolak DW, Sun RY, 2017a. Air-ground channel characterization for unmanned aircraft systems. Part I: methods, measurements, and models for over-water settings. *IEEE Trans Veh Technol*, 66(1):26-44. https://doi.org/10.1109/TVT.2016.2530306

Matolak DW, Sun RY, 2017b. Air-ground channel characterization for unmanned aircraft systems. Part III: the suburban and near-urban environments. *IEEE Trans Veh Technol*, 66(8):6607-6618. https://doi.org/10.1109/TVT.2017.2659651

Matolak DW, Sen I, Xiong WH, et al., 2005. 5 GHz wireless channel characterization for vehicle to vehicle communications. IEEE Military Communications Conf, p.3016-3022. https://doi.org/10.1109/MILCOM.2005.1606122

Meredith J, 2016. Study on Channel Model for Frequency Spectrum above 6 GHz. Technical Report TR 38900, 3GPP.

Miaoudakis A, Lekkas A, Kalivas G, et al., 2005. Radio channel characterization in industrial environments and spread spectrum modem performance. IEEE Conf on Emerging Technologies and Factory Automation, p.87-93. https://doi.org/10.1109/ETFA.2005.1612506

Molisch AF, 2012. Wireless Communications. John Wiley & Sons, New York.

Moral PD, 1996. Non-linear filtering: interacting particle resolution. *Markov Process Rel Field*, 2(4):555-581.

Nachmani E, Marciano E, Burshtein D, et al., 2017. RNN decoding of linear block codes. https://arxiv.org/abs/1702.07560

Nachmani E, Marciano E, Lugosch L, et al., 2018. Deep learning methods for improved decoding of linear codes. *IEEE J Sel Top Signal Process*, 12(1):119-131. https://doi.org/10.1109/JSTSP.2017.2788405

Navabi S, Wang CW, Bursalioglu OY, et al., 2018. Predicting wireless channel features using neural networks. IEEE Int Conf on Communications, p.1-6. https://doi.org/10.1109/ICC.2018.8422221

Newhall WG, Mostafa R, Dietrich C, et al., 2003. Wideband air-to-ground radio channel measurements using an antenna array at 2 GHz for low-altitude operations. IEEE Military Communications Conf, p.1422-1427. https://doi.org/10.1109/MILCOM.2003.1290436

Nikolaidis V, Moraitis N, Kanatas AG, 2016. Dual polarized MIMO LMS channel measurements and characterization in a pedestrian environment. 10th European Conf on Antennas and Propagation, p.1-5. https://doi.org/10.1109/EuCAP.2016.7481470

Ono F, Takizawa K, Tsuji H, et al., 2015. S-band radio propagation characteristics in urban environment for unmanned aircraft systems. Int Symp on Antennas and Propagation, p.1-4.

O'Shea TJ, Hoydis J, 2017. An introduction to machine learning communications systems. https://arxiv.org/abs/1702.00832v1

Petropoulou P, Michailidis ET, Panagopoulos AD, et al., 2014. Radio propagation channel measurements for multi-antenna satellite communication systems: a survey. *IEEE Antenn Propag Mag*, 56(6):102-122. https://doi.org/10.1109/MAP.2014.7011023

Piesiewicz R, Kleine-Ostmann T, Krumbholz N, et al., 2005. Terahertz characterisation of building materials. *Electron Lett*, 41(18):1002-1004. https://doi.org/10.1049/el:20052444

Piesiewicz R, Jacob M, Koch M, et al., 2008. Performance analysis of future multigigabit wireless communication systems at THz frequencies with highly directive antennas in realistic indoor environments. *IEEE J Sel Top Quant Electron*, 14(2):421-430. https://doi.org/10.1109/JSTQE.2007.910984

Pometcu L, D'Errico R, 2018. Large scale and clusters characteristics in indoor sub-THz channels. Proc 29th Annual Int Symp Personal Indoor and Mobile Radio Communications, p.1405-1409. https://doi.org/10.1109/PIMRC.2018.8580938

Priebe S, Kuerner T, 2013. Stochastic modeling of THz indoor radio channels. *IEEE Trans Wirel Commun*, 12(9):4445-4455. https://doi.org/10.1109/TWC.2013.072313.121581

Priebe S, Jastrow C, Jacob M, et al., 2011. Channel and propagation measurements at 300 GHz. *IEEE Trans Antenn Propag*, 59(5):1688-1698. https://doi.org/10.1109/TAP.2011.2122294

Priebe S, Kannicht M, Jacob M, et al., 2013. Ultra broadband indoor channel measurements and calibrated ray tracing propagation modeling at THz frequencies. *J Commun Netw*, 15(6):547-558. https://doi.org/10.1109/JCN.2013.000103

Priebe S, Jacob M, Kuerner T, 2014. Angular and RMS delay spread modeling in view of THz indoor communication systems. *Radio Sci*, 49(3):242-251. https://doi.org/10.1002/2013RS005292

Quinlan JR, 1986. Induction of decision trees. *Mach Learn*, 1(1):81-106.

Raimundo X, Salous S, Cheema A, 2018. Indoor dual polarised radio channel characterisation in the 54 and 70 GHz bands. *IET Microw Antenn Propag*, 12(8):1287-1292. https://doi.org/10.1049/iet-map.2017.0711

Rappaport TS, McGillem CD, 1987. Characterising the UHF factory radio channel. *Electron Lett*, 23(19):1015-1017. https://doi.org/10.1049/el:19870712

Rappaport TS, Xing YC, MacCartney GR, et al., 2017. Overview of millimeter wave communications for fifth-generation (5G) wireless networks: with a focus on propagation models. *IEEE Trans Antenn Propag*, 65(12):6213-6230. https://doi.org/10.1109/TAP.2017.2734243

Rasmussen CE, 2003. Gaussian processes in machine learning. In: Bousquet O, Luxburg U, Rätsch G (Eds.), Advanced Lectures on Machine Learning. Springer Berlin Heidelberg, p.63-71. https://doi.org/10.1007/978-3-540-28650-9_4

Rey S, Eckhardt JM, Peng B, et al., 2017. Channel sounding techniques for applications in THz communications: a first correlation based channel sounder for ultra-wideband dynamic channel measurements at 300 GHz. Proc 9$^{th}$ Int Congress on Ultra Modern Telecommunications and Control Systems and Workshops, p.449-453. https://doi.org/10.1109/ICUMT.2017.8255203

Richter F, Fehske AJ, Fettweis GP, 2009. Energy efficiency aspects of base station deployment strategies for cellular networks. IEEE 70$^{th}$ Vehicular Technology Conf, p.1-5. https://doi.org/10.1109/VETECF.2009.5379031

Rieche M, Ihlow A, Arndt D, et al., 2015. Modeling of the land mobile satellite channel considering the terminal's driving direction. *Int J Antenn Propag*, 2015:372124. https://doi.org/10.1155/2015/372124

Samimi MK, Rappaport TS, MacCartney GR, 2015. Probabilistic omnidirectional path loss models for millimeter-wave outdoor communications. *IEEE Wirel Commun Lett*, 4(4):357-360. https://doi.org/10.1109/LWC.2015.2417559

Series M, 2015. IMT Vision-Framework and Overall Objectives of the Future Development of IMT for 2020 and Beyond. Report M.2083-0, ITU-R, Geneva, Switzerland.

Sexton D, Mahony M, Lapinski M, et al., 2005. Radio channel quality in industrial wireless sensor networks. Sensors for Industry Conf, p.88-94. https://doi.org/10.1109/SICON.2005.257875

Shafin R, Liu LJ, Chandrasekhar V, et al., 2019. Artificial intelligence-enabled cellular networks: a critical path to beyond-5G and 6G. https://arxiv.org/abs/1907.07862

Simunek M, Pechac P, Fontan FP, 2011. Excess loss model for low elevation links in urban areas for UAVs. *Radioengineering*, 20(3):561-568.

Solomitckii D, Orsino A, Andreev S, et al., 2018. Characterization of mmWave channel properties at 28 and 60 GHz in factory automation deployments. IEEE Wireless Communications and Networking Conf, p.1-6. https://doi.org/10.1109/WCNC.2018.8377337

Strinati EC, Barbarossa S, Gonzalez-Jimenez JL, et al., 2019. 6G: the next frontier. https://arxiv.org/abs/1901.03239

Sun RY, Matolak DW, 2017. Air-ground channel characterization for unmanned aircraft systems. Part II: hilly and mountainous settings. *IEEE Trans Veh Technol*, 66(3):1913-1925. https://doi.org/10.1109/TVT.2016.2585504

Tang P, Zhang J, Molisch AF, et al., 2018. Estimation of the $K$-factor for temporal fading from single-snapshot wideband measurements. *IEEE Trans Veh Technol*, 68(1):49-63. https://doi.org/10.1109/TVT.2018.2878352

Tanghe E, Joseph W, Verloock L, et al., 2008. The industrial indoor channel: large-scale and temporal fading at 900, 2400, and 5200 MHz. *IEEE Trans Wirel Commun*, 7(7):2740-2751. https://doi.org/10.1109/TWC.2008.070143

Tu HD, Shimamoto S, 2009. A proposal of wide-band air-to-ground communication at airports employing 5-GHz band. IEEE Wireless Communications and Networking Conf, p.1-6. https://doi.org/10.1109/WCNC.2009.4917538

Vogel WJ, Goldhirsh J, 1986. Tree attenuation at 869 MHz derived from remotely piloted aircraft measurements. *IEEE Trans Antenn Propag*, 34(12):1460-1464. https://doi.org/10.1109/TAP.1986.1143781

Vogel WJ, Goldhirsh J, 1988. Fade measurements at L-band and UHF in mountainous terrain for land mobile satellite systems. *IEEE Trans Antenn Propag*, 36(1):104-113. https://doi.org/10.1109/8.1081

Vogel WJ, Goldhirsh J, 1993. Earth-satellite tree attenuation at 20 GHz: foliage effects. *Electron Lett*, 29(18):1640-1641. https://doi.org/10.1049/el:19931092

Wang CX, Bian J, Sun J, et al., 2018. A survey of 5G channel measurements and models. *IEEE Commun Surv Tutor*, 20(4):3142-3168. https://doi.org/10.1109/COMST.2018.2862141

Wang Z, Li L, Xu Y, et al., 2018. Handover control in wireless systems via asynchronous multiuser deep reinforcement learning. *IEEE Int Thing J*, 5(6):4296-4307. https://doi.org/10.1109/JIOT.2018.2848295

Wang ZY, Shen C, 2017. Small cell transmit power assignment based on correlated bandit learning. *IEEE J Sel Area Commun*, 35(5):1030-1045. https://doi.org/10.1109/JSAC.2017.2679660

Watkins C, 1989. Learning from Delayed Rewards. PhD Thesis, University of Cambridge, Cambridge, UK.

Wentz M, Stojanovic M, 2015. A MIMO radio channel model for low-altitude air-to-ground communication systems. IEEE 82$^{nd}$ Vehicular Technology Conf, p.1-6. https://doi.org/10.1109/VTCFall.2015.7390797

Willink TJ, Squires CC, Colman GW, et al., 2015. Measurement and characterization of low-altitude air-to-ground MIMO channels. *IEEE Trans Veh Technol*, 65(4):2637-2648. https://doi.org/10.1109/TVT.2015.2419738

WP5D I, 2017. Guidelines for Evaluation of Radio Interface Technologies for IMT-2020. Report M.2412, ITU-R, Geneva, Switzerland.

Xie YJ, Fang YG, 2000. A general statistical channel model for mobile satellite systems. *IEEE Trans Veh Technol*, 49(3):744-752. https://doi.org/10.1109/25.845094

Yang GS, Zhang Y, He ZW, et al., 2019. Machine-learning-based prediction methods for path loss and delay spread in air-to-ground millimetre-wave channels. *IET Microw Antenn Propag*, 13(8):1113-1121. https://doi.org/10.1049/iet-map.2018.6187

Yanmaz E, Kuschnig R, Bettstetter C, 2011. Channel measurements over 802.11a-based UAV-to-ground links. IEEE GLOBECOM Workshops, p.1280-1284. https://doi.org/10.1109/GLOCOMW.2011.6162389

Zhang C, Hui YN, 2011. Broadband air-to-ground communications with adaptive MIMO datalinks. IEEE/AIAA 30th Digital Avionics Systems Conf, p.4D4-1. https://doi.org/10.1109/DASC.2011.6095912

Zhang J, 2016. The interdisciplinary research of big data and wireless channel: a cluster-nuclei based channel model. *China Commun*, 13(S2):14-26. https://doi.org/10.1109/CC.2016.7833457

Zhang J, Pan C, Pei F, et al., 2014. Three-dimensional fading channel models: a survey of elevation angle research. *IEEE Commun Mag*, 52(6):218-226. https://doi.org/10.1109/MCOM.2014.6829967

Zhang JH, Tang P, Tian L, et al., 2017a. 6–100 GHz research progress and challenges for fifth generation (5G) and future wireless communication from channel perspective. *Sci China Inform Sci*, 60(8):080301. https://doi.org/10.1007/s11432-016-9144-x

Zhang JH, Zhang YX, Yu YW, et al., 2017b. 3D MIMO: how much does it meet our expectations observed from channel measurements? *IEEE J Sel Areas Commun*, 35(8):1887-1903. https://doi.org/10.1109/JSAC.2017.2710758

Zhang JH, Zheng Z, Zhang YX, et al., 2018. 3D MIMO for 5G NR: several observations from 32 to massive 256 antennas based on channel measurement. *IEEE Commun Mag*, 56(3):62-70. https://doi.org/10.1109/MCOM.2018.1700846

Zhang P, Niu K, Tian H, et al., 2019. The outlook for 6G mobile communication technologies. *J Commun*, 4(1):145-152.